Modeling of InGaN/Si tandem cells: comparison between 2-contacts/4-contacts

Walid El-Huni, Anne Migan-Dubois, David Alamarguy, Zakaria Djebbour

EPJ Photovoltaics **8**, 85502 (2017)
www.epj-pv.org
DOI: 10.1051/epjpv/2017003

Modeling of InGaN/Si tandem cells: comparison between 2-contacts/4-contacts

Walid El-Huni[1,2,a], Anne Migan[1,2], David Alamarguy[1], and Zakaria Djebbour[1,3]

[1] GeePs, UMR 8507, CNRS, Centrale Supélec, UPsud, UPMC, 11 Rue Joliot-Curie, 91192 Gif-sur-Yvette Cedex, France
[2] Université Pierre et Marie Curie, UPMC, 4 Place Jussieu, 75005 Paris, France
[3] Département des Sciences Physiques, UVSQ, 45 Avenue des États-Unis, 78035 Versailles, France

Received: 18 November 2016 / Received in final form: 4 January 2017 / Accepted: 26 January 2017

Abstract Due to its electrical and optical interesting properties, InGaN alloy is being intensively studied to be combined with silicon in order to achieve low-cost high-efficiency solar cell. However, a relatively thick monophasic layer of InGaN is difficult to grow due to the relaxation issue in material. This issue can be avoided by semibulk structure. In this work, we present an InGaN/Si double-junction solar cell modeled using Silvaco-ATLAS TCAD software. We have taken into account polarization effect in III-N materials. We have shown that 50% of indium is needed to ensure the current matching between the top cell and the bottom cell in 2-terminal configuration. Such high indium composition is technologically challenging to grow. Thus, we have modeled a 4-terminals solar cell with relatively low indium composition (In = 25%) where current matching is not needed. With technologically feasible structural parameters, we have shown that an efficiency near to 30% can be achieved with InGaN/Si 4-contact tandem cell.

1 Introduction

Silicon-based tandem solar cell is a promising design for low-cost high-efficiency solar cell. However, it is hard to find a matched-bandgap material with silicon (1.7–1.8 eV) [1]. The maximum power conversion efficiency (PCE) for a tandem solar cell is 31.6% for GaInP/GaAs tandem cell [2]. While GaAs is more expensive compared to silicon (Si). For this reason, many groups have tried to combine III–V material with Si. The record of Si-based tandem solar cell is the one achieved recently with a PCE of 29.8% [3].

InGaN material has been intensively studied last years to be used for photovoltaic applications. This alloy has a wide-range direct bandgap that varies from 0.7 eV (InN) to 3.4 eV (GaN) [4,5]. Its high absorption coefficient [6], allows the use of very thin layer (<1 μm) to absorb the majority of incident light. They are more resistant to high-energetic radiations which is beneficial to spacial uses [7].

These advantages make InGaN material interesting for PV applications. However, InGaN-based solar cell has a maximum PCE of 6% [8]. One of the most important challenges that limits the performance of this material is the growth of high-quality relatively-thick InGaN layer. Due to large lattice mismatch between InN and GaN, InGaN grown layer start to relax through dislocation defects after a certain thickness, called critical thickness [9,10]. This critical thickness depends on indium composition to the extend that at 30% of indium the critical thickness is less than 10 nm [11,12].

However, a solution that has been initiated by Pantzas et al. [9] in order to avoid the relaxation issue, which is semibulk structure. This structure is obtained by periodically stopping the indium flux, during the growth process, before arriving to the critical thickness. This will lead to the introduction of GaN interlayers. We have previously shown the enhancement of InGaN-based solar cell's performance using semibulk structure [13].

In this work, we aim to study the integration of InGaN-based semibulk-structured solar cell with Si-based solar cell for high-efficiency tandem cell.

2 Methode

We have used SILVACO-Atlas for our simulations. SILVACO-Atlas is a finite-element physical-based simulation tool, which solves the three equations: Poisson equation, continuity equations, and transport equations at each node. In this section we explain some of physical models that have been used in our simulations. Parameters' values are listed in Table 1.

[a] e-mail: walid.elhuni@geeps.centralesupelec.fr

Table 1. Parameters used in simulations.

Parameter	[Unit]	c-Si	GaN	InN	Interpolation (InGaN)
a	[Å]	5.43	3.189	3.545	Linear
E_g	[eV]	1.08	3.42	0.76	Bowing = 1
			Recombination		
τ_{n0}	[s]	1, 3e-3	5e-9	5e-9	
τ_{p0}	[s]	1, 3e-3	5e-9	5e-9	
C_{rad}	[cm^3/s]		1e-8	1e-8	
S_n	[cm/s]	100	1e4		
S_p	[cm/s]	100	1e4		
			Mobility		
μ_{1n}	[cm^2/(V s)]	55.24	55	30	Linear
μ_{2n}	[cm^2/(V s)]	1429.23	1000	1100	Linear
N_{gn}	[cm^{-3}]	1.07e17	2e17	8e18	Linear
μ_{1p}	[cm^2/(V s)]	49.7	3	3	
μ_{2p}	[cm^2/(V s)]	479.37	170	340	Linear
N_{gp}	[cm^{-3}]	1.6e17	3e17	3e17	
			Polarization		
P_{sp}	[C/m^2]		–0.034	–0.042	Bowing = –0.037
e_{33}	[C/m^2]		0.73	0.97	Linear
e_{31}	[C/m^2]		–0.49	–0.57	Linear
C_{33}	[GPa]		398	224	Linear
C_{31}	[GPa]		106	92	Linear

2.1 Electrons and holes mobilities

For electrons and holes mobilities, we have chosen concentration-dependent mobility:

$$\mu_{n0}(\mathrm{cm^2\ V^{-1}\ s^{-1}}) = \mu_{1n} + \frac{\mu_{2n} - \mu_{1n}}{1 + (N/N_{gn})^{\delta_n}} \quad (1)$$

$$\mu_{p0}(\mathrm{cm^2\ V^{-1}\ s^{-1}}) = \mu_{1p} + \frac{\mu_{2p} - \mu_{1p}}{1 + (N/N_{gp})^{\delta_p}} \quad (2)$$

where μ_1 and μ_2 are the minimum and maximum mobilities, N is the impurity local concentration, N_g and δ are fitting parameters.

2.2 Recombination processes

Two recombination processes are considered here: the radiative recombination and the Schokley-Read-Hall recombination (SRH):
Radiative recombination is given by:

$$R_{np}^{opt}(\mathrm{cm^{-3}\ s^{-1}}) = C^{opt}(np - n_{ie}^2); \quad (3)$$

and Schokley-Read-Hall recombination (SRH), which is a non-radiative recombination, is given by:

$$R_{srh}(\mathrm{cm^{-3}\ s^{-1}}) = \frac{pn - n_{ie}^2}{\tau_p[n + n_{ie}] + \tau_n[p + n_{ie}]} \quad (4)$$

where n and p are electron and hole concentrations, respectively, n_{ie} is the intrinsic concentration, τ_n and τ_p are electron and hole lifetimes, respectively. For silicon-based solar cell, we have taken into account the dependancy of carriers' lifetime on doping concentration. Surface recombination has been included in our simulations using surface velocity parameters S_n and S_p for electrons and holes respectively.

2.3 Bandgap

The bandgap, E_g, is calculated using Vegard's law:

$$E_g^{\mathrm{In}_x\mathrm{Ga}_{1-x}\mathrm{N}}(\mathrm{eV}) = xE_g^{\mathrm{InN}} + (1-x)E_g^{\mathrm{GaN}} - bx(1-x) \quad (5)$$

where x is the indium composition and b is the bowing parameter.

2.4 Polarization

III-nitrides are polar materials due to the non-centrosymmetric nature of their crystallographic structure. This causes a spontaneous polarization, P_{sp}, that can be calculated for InGaN by:

$$P_{sp}^{\mathrm{In}_x\mathrm{Ga}_{1-x}\mathrm{N}}(\mathrm{C/m^2}) = xP_{sp}^{\mathrm{InN}} + (1-x)P_{sp}^{\mathrm{GaN}} - bx(1-x). \quad (6)$$

In addition, due to the lattice difference between the InGaN epilayer and the GaN substrate, the strain causes a piezoelectric-induced polarization, P_{pz}, that can be calculated by:

$$P_{pz}^{(\mathrm{In}_x\mathrm{Ga}_{1-x}\mathrm{N})}(\mathrm{C/m^2}) = 2 \times R_s\left(e_{31}(x) - \frac{C_{13}(x)}{C_{33}(x)}e_{33}(x)\right)\epsilon(x) \quad (7)$$

$$\epsilon(x) = (a - a_0)/a_0 \quad (8)$$

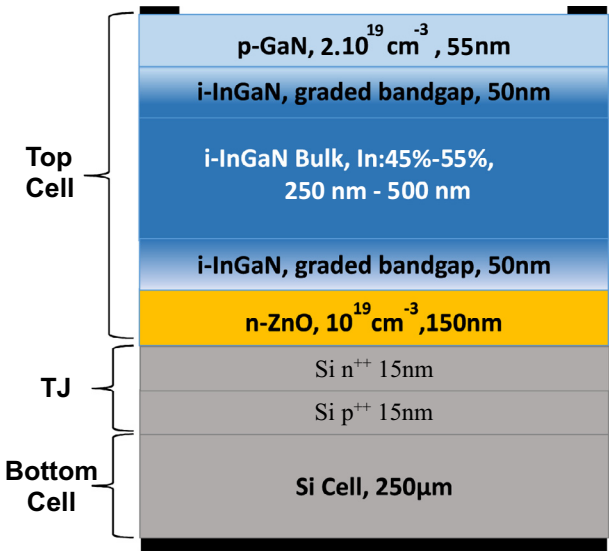

Fig. 1. Modeled structure for InGaN/Si 2-terminal tandem cell. Top cell structure is based on the work of reference [15], and bottom cell structure is based on the work of reference [23].

where R_s is the residual strain. $R_s = 1$ means that the layer is fully strained. a_0 and a are the initial and stressed lattice constants. The total polarization is the sum of both spontaneous polarization and piezoelectric polarization, taking into account the direction of each.

3 Results

In these simulations we have taken into account the attenuation of polarization effect as the number of periods increases as demonstrated experimentally by Bai et al. [14]. We have also lowered the carriers' lifetime in p-GaN layer as it shows lower external quantum efficiency (EQE) [15] for lower wavelengths. A bowing parameter of 1 has been used for bandgap calculation. We have used the same value to calculate electron affinity for InGaN, while the maximum valence band varies linearly [16]. More details about the physical and optical models can be found in our previous work [17]. We have also, in the latter work, validated our model by comparing our simulation results to experimental results obtained by other groups [15,18,19], for both InGaN-based top cell and Si-based bottom cell.

First, we show the modeling results for a 2-terminal InGaN/Si tandem cell. The modeled structure is shown in Figure 1. Due to the thermal budget to grow InGaN material, it is not preferable to grow it directly on Si-based junction, because this will deteriorate the tunneling junction which is embedded in Si. For this reason, we have added a ZnO intermediate layer in the modeled structure.

As we expect that the optimum would be obtained with high indium composition, which is necessary to fulfill the current-matching condition, we have assumed a bulk absorbing layer of InGaN in order to avoid the high barriers that would be caused by semibulk structure. We have also used a graded heterojunctions in both sides of intrinsic layer in order to ensure the band continuity at interfaces. For Si-based bottom cell, the top cell bandgap should be between 1.7 and 1.8 eV in order to achieve the current matching [1]. For this reason, we have varied the indium composition from 45% to 55%. Using SILAVCO-ATLAS TCAD software, we have optimized this structure and we show, in Figure 2, that the maximal efficiency of about 28% is obtained with 50% of indium and with 400-nm thickness of InGaN absorbing layer. These values, which are needed to fulfill the current-matching condition and to extract the optimal photogenerated current density, are not technologically attainable today.

Using XPS analysis, we have studied the interface between ZnO and Si. Figure 3 shows the atomic concentration for detected elements in function of sputter time. According to energy positions, we have distinguished between the oxygen (O) that is related to Zn and the O that is related to Si. We did the same for Si. The ZnO was grown using PLD (Pulsed Laser Deposition) with a thickness of 12 nm. Based on a reference sample of SiO_2, we have estimated thickness of SiO_x between ZnO and Si to be about 3 nm $\pm$ 0.5 nm. Introducing this interafacial layer in the modeled structure, we show that beyond 2 nm of thickness the PCE start to decrease dramatically to extend that at 3 nm of SiO_x thickness, we do not expect to have a PV response. This is because of the high bandgap of SiO_x that prevents the tunneling process through the tunneling junction. Figure 4 shows the dependence of PCE in function of SiO_x thickness.

Due to the difficulty of achieving a 2-terminal InGaN/Si tandem cell, at least for short-term, we need to study another alternative which is 4-terminal design. The advantage of this design is that it does not require a current matching between top and bottom cell. Consequently, it offers a larger range of bandgaps combination. It has been shown also that 4-terminal design is less sensitive to the variation of solar spectrum during the day [20] and, hence, it has a higher daily-energy yield compared to 2-terminal design.

Consequently, we have modeled 4-terminal InGaN/Si tandem cell shown in Figure 5. For bottom cell we have used Si-based PERL-structured solar cell. For top cell we have used InGaN-based semibulk-structured solar cell, with GaN interlayers of 2 nm. We have taken into account the polarization effect of the InGaN. We have varied the indium composition from 20% to 30%, and the number of periods from 10 to 25. The InGaN sublayers thickness was varied from 5 nm to 20 nm. Figure 6 shows the results of total PCE. One can see that the optimum is obtained at 25% of indium with number of periods between 20 and 25. The reason of having the optimum at higher number of periods is because that we have taken into account the attenuation of polarization effect with increasing number of periods. However, the InGaN-sublayer thickness should be more than 10 nm in order to have the maximum efficiency of about 27%. However, the critical thickness of InGaN at 25% of indium provided by some models is less than 10 nm [11,21]. At 30% of indium composition, PCE

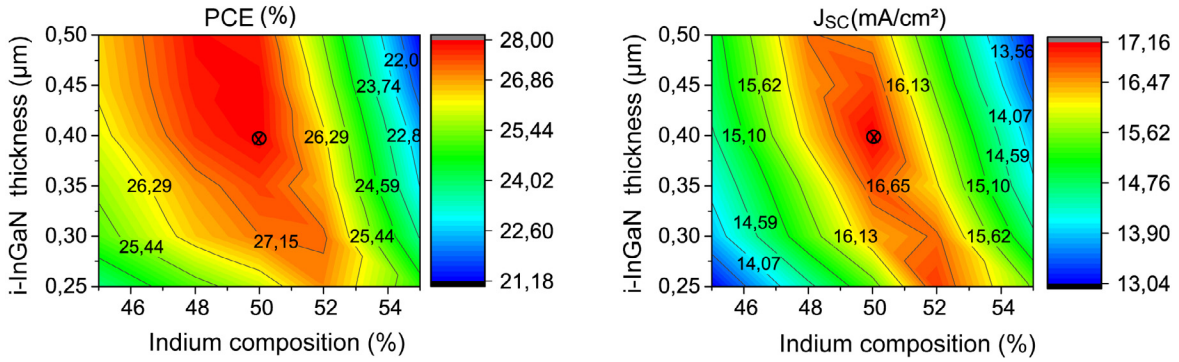

Fig. 2. PCE (left) and J_{sc} (right) of InGaN/Si 2-terminal tandem cell as a function of indium composition and i-InGaN thickness of InGaN-based top cell.

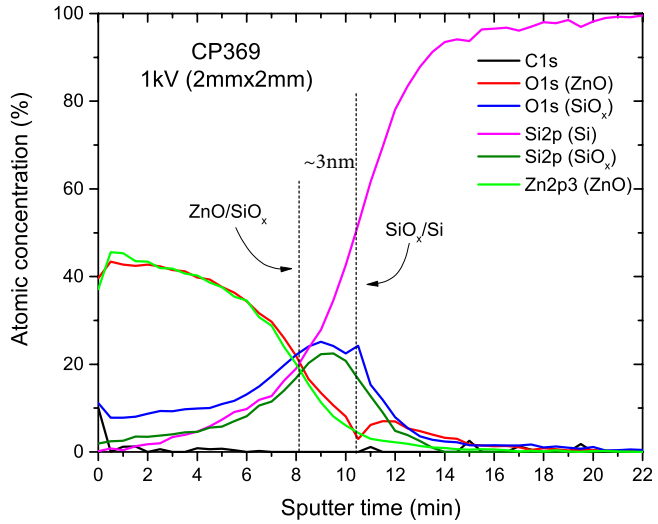

Fig. 3. XPS depth profiles of Zn, O and Si, as a function of sputtering time. We have decomposed the O related to Si and the O related to Zn. We have done the same for Si.

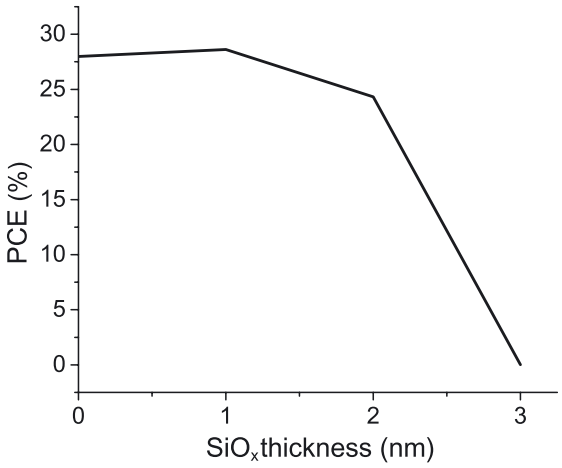

Fig. 4. PCE of InGaN/Si 2-terminal tandem cell as a function of SiO_x interfacial layer thickness.

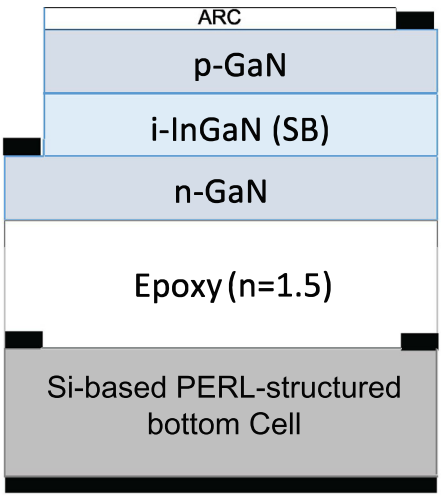

Fig. 5. Modeled structure of InGaN/Si 4-terminal tandem cell.

decreases. This is because of barriers' height that become more important which decreases the tunneling probability.

We have considered the dichroic mirror (DM) that has been demonstrated experimentally by Young et al. [22], which has a reflectance of 89% in the region coinciding with the InGaN photoresponse (365–460 nm). At wavelengths beyond 470 nm, the reflectance average is about 4.0% only. If we take into account the effect of this mirror in our simulations, we show that, in Figure 7, the InGaN-sublayer optimal thickness can be reduced to 5 nm, which is less than or in the same order of magnitude of the critical thickness. We show also that efficiencies around 27% can be obtained with only 20% of indium.

For both with and without DM, we noticed that the structure with 30% of indium is more sensitive to the variation of number of periods. This is explained by the fact that at 30% of indium, the polarization-induced charges at the interfaces increases, which increases the opposite electric field in barriers. As the polarization effect decreases with the increase of number of periods, one can notice the enhancement in PCE for higher number of periods.

4 Conclusion

Using a realistic modeling, we have shown that InGaN/Si 2-terminal tandem cell is technologically challenging due to the need of high-indium composition

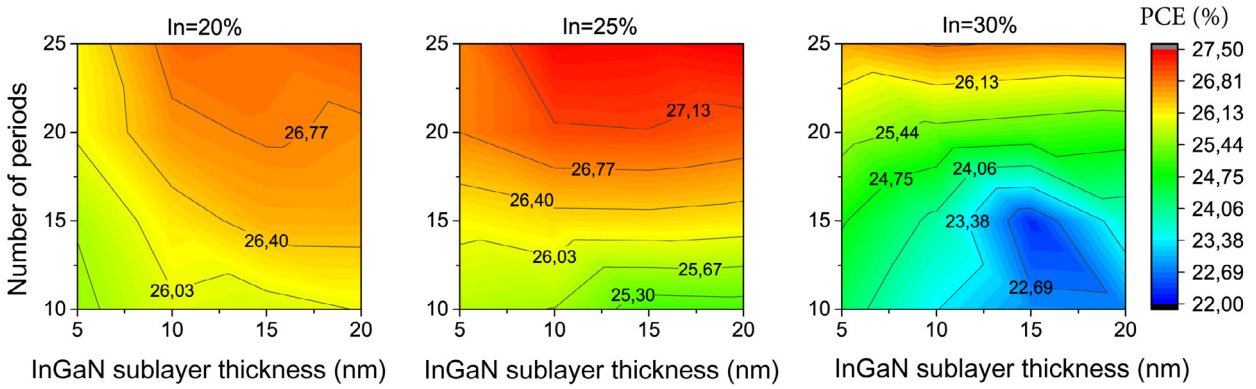

Fig. 6. PCE of InGaN/Si 4-terminal tandem cell as a function of InGaN sublayers' thickness and number of periods. The indium composition has been varied for 20%, 25% and 30%.

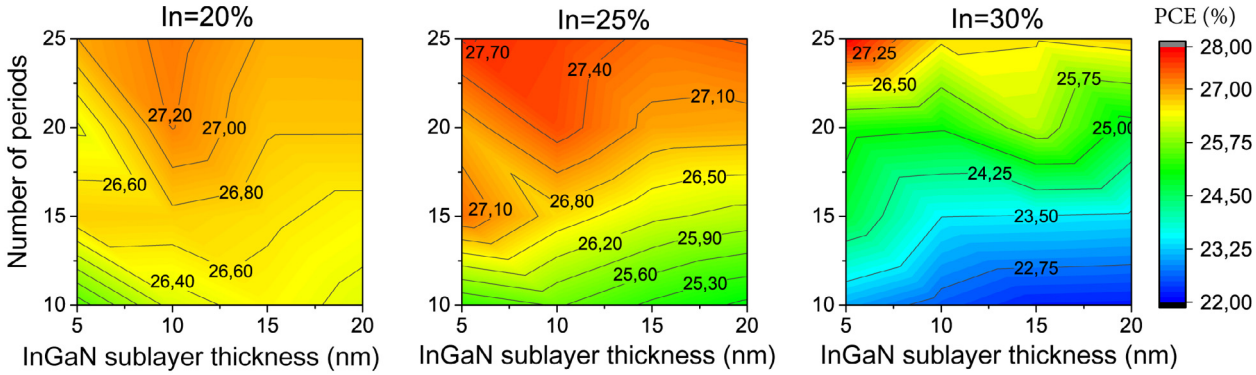

Fig. 7. PCE of InGaN/Si 4-terminal tandem cell as a function of InGaN sublayers' thickness and number of periods. The indium composition has been varied for 20%, 25% and 30%. We have taken into account the DM at the back side of top cell.

(about 50%) and relatively thick absorbing layer (near 400 nm), in order to fulfill the current-matching condition. We have shown also that the SiO_x layer at the interface between ZnO and Si will deteriorate the PCE of the 2-terminal tandem cell.

However, a 4-terminal design has shown a good performance for other junctions and has the advantage of not requiring a current-matching between top and bottom cells. We have shown that InGaN/Si 4-terminal tandem cell can achieve a PCE near to 30%, taking into account a realistic and feasible structural parameters.

This work has been supported by the French National Research Agency (ANR) under the NOVAGAINS contract ANR-12-PRGE-0014-01.

References

1. F. Meillaud, A. Shah, C. Droz, E. Vallat-Sauvain, C. Miazza, Sol. Energy Mater. Sol. Cells **90**, 2952 (2006)
2. R. Kapusta, Press release: Alta Devices Achieves 31.6% Solar Energy Efficiency Record; Changes the Fundamental Economics for Unmanned Aerial Vehicles (2016)
3. J. Bebon, Press release: NREL, CSEM Jointly Set New Efficiency Record with Dual-Junction Solar Cell (2015)
4. I. Vurgaftman, J.R. Meyer, L.R. Ram-Mohan, J. Appl. Phys. **89**, 5815 (2001)
5. I. Vurgaftman, J.R. Meyer, J. Appl. Phys. **94**, 3675 (2003)
6. J. Wu, W. Walukiewicz, K.M. Yu, J.W. Ager, E.E. Haller, H. Lu, W.J. Schaff, Appl. Phys. Lett. **80**, 4741 (2002)
7. J. Wu, W. Walukiewicz, K.M. Yu, W. Shan, J.W. Ager, E.E. Haller, H. Lu, W.J. Schaff, W.K. Metzger, S. Kurtz, J. Appl. Phys. **94**, 6477 (2003)
8. B.W. Liou, Thin Solid Films **520**, 1 (2011)
9. K. Pantzas, Y. El Gmili, J. Dickerson, S. Gautier, L. Largeau, O. Mauguin, G. Patriarche, S. Suresh, T. Moudakir, C. Bishop, A. Ahaitouf, T. Rivera, C. Tanguy, P. Voss, A. Ougazzaden, J. Cryst. Growth **370**, 57 (2013)
10. D. Holec, Y. Zhang, D.V.S. Rao, M.J. Kappers, C. McAleese, C.J. Humphreys, J. Appl. Phys. **104**, 12 (2008)
11. D. Holec, P.M.F.J. Costa, M.J. Kappers, C.J. Humphreys, J. Cryst. Growth **303**, 314 (2007)
12. S. Srinivasan, L. Geng, R. Liu, F.A. Ponce, Y. Narukawa, S. Tanaka, Appl. Phys. Lett. **83**, 5187 (2003)
13. M. Arif, W. Elhuni, J. Streque, S. Sundaram, S. Belahsene, Y. El Gmili, M. Jordan, X. Li, G. Patriarche, A. Slaoui, A. Migan, R. Abderrahim, Z. Djebbour, P. Voss, J. Salvestrini, A. Ougazzaden, Sol. Energy Mater. Sol. Cells **159**, 405 (2017)
14. J. Bai, T. Wang, S. Sakai, J. Appl. Phys. **90**, 1740 (2001)

15. N.G. Young, R.M. Farrell, Y.L. Hu, Y. Terao, M. Iza, S. Keller, S.P. DenBaars, S. Nakamura, J.S. Speck, Appl. Phys. Lett. **103**, 173903 (2013)
16. P.G. Moses, C.G. Van De Walle, Appl. Phys. Lett. **96**, 2 (2010)
17. W. El-Huni, A. Migan, Z. Djebbour, J.-P. Salvestrini, A. Ougazzaden, Prog. Photovolt.: Res. Appl. **24**, 11 (2016)
18. J. Zhao, A. Wang, M.A. Green, Prog. Photovolt.: Res. Appl. **7**, 471 (1999)
19. J. Zhao, A. Wang, M.A. Green, Solar Energy Mater. Sol. Cells **66**, 27 (2001)
20. H. Liu, Z. Ren, Z. Liu, A.G. Aberle, T. Buonassisi, I.M. Peters, Opt. Express **23**, A382 (2015)
21. W. Zhao, L. Wang, J. Wang, Z. Hao, Y. Luo, J. Cryst. Growth **327**, 202 (2011)
22. N.G. Young, E.E. Perl, R.M. Farrell, M. Iza, S. Keller, J.E. Bowers, S. Nakamura, S.P. DenBaars, J.S. Speck, Appl. Phys. Lett. **104**, 163902 (2014)
23. A. Lanterne, J. Le Perchec, S. Gall, M. Coig, A. Tauzin, Y. Veschetti, Energy Procedia **55**, 437 (2014)

Cite this article as: Walid El-Huni, Anne Migan, David Alamarguy, Zakaria Djebbour, Modeling of InGaN/Si tandem cells: comparison between 2-contacts/4-contacts, EPJ Photovoltaics **8**, 85502 (2017).